Open Access

Catalysis Research

LIDSEN Publishing Inc.

Original Research

Hydrocracking of Di-and Triaromatic Hydrocarbons to Monoaromatics over Mixed Bi-functional Catalysts

Anilkumar Mettu *, Ninad Loke, Vilas Patil, Rahul Panday, Sreenivasarao Gajula

SABIC Research and Technology Pvt. Ltd, Chikkadunnasandra, Anekal Taluk, Off. Sarjapura - Attibele State Highway, Bangalore, Karnataka 562125, India; E-Mail: anil.mettu@sabic.com; Ninadloke@gmail.com; vilas.patil@sabic.com; Rahul.pandey515@gmail.com; sreenivasa.rao@sabic.com

* **Correspondence:** Anilkumar Mettu; E-Mail: anil.mettu@sabic.com

Academic Editors: Angela Martins and Antonio Chica

Special Issue: Zeolite Materials and Catalysis

Catalysis Research
2022, volume 2, issue 3
doi:10.21926/cr.2203021

Received: January 10, 2022
Accepted: June 17, 2022
Published: July 19, 2022

Abstract

In this study, we present selective hydrocracking of poly (di and tri) aromatic compounds to monoaromatics, such as benzene, toluene, and xylenes (BTX), over a mixture of Pt/Al_2O_3 and Y zeolites. The polyaromatic compounds feed is a combined simulated model feed, which is similar to light cycle oil (LCO) in composition. The feed is processed in a fixed bed reactor over a catalyst mixture: in the first step, selective hydrogenation of di and tri-aromatic compounds occurs in the presence of Pt/Al_2O_3 catalyst, followed by conversion of selective hydrocracking of partial hydrogenated polyaromatic hydrocarbons into BTX-rich stream over Y zeolite. The structural properties and Pt dispersion of Pt/Al_2O_3 were studied by X-ray powder diffraction (XRD) and high-angle annular dark-field scanning transmission electron microscopy (HAADF-STEM). The acidity of Y zeolite with different SiO_2/Al_2O_3 ratios (SAR) was studied by temperature-programmed desorption of NH_3 (NH_3-TPD). In addition, the textural properties of catalysts were determined using the N_2 adsorption and desorption method. Different parameters such as the effect of temperature, effect of weight hourly space velocity (WHSV), different SAR of Y zeolite, Pt/Al_2O_3, and Y zeolite wt% ratios, and paraffin concentration were

investigated. The maximum BTX yield of ~28 wt.% was obtained at 450°C, WHSV-0.7 h^{-1}, H_2 pressure 60 bar, Pt/Al_2O_3, and Y zeolite ratios of 1:2 (wt%) at Y zeolite SAR of 80. These results suggest that the yield of BTX strongly depends on the hydrogenation function (Pt/Al_2O_3) and acidity function of Y zeolite. Furthermore, the concentration of paraffin plays a key role in the conversion of diaromatics and triaromatics and desired products of BTX formation.

Keywords
Light cycle oil (LCO); poly aromatic compounds; hydrogenation; hydrocracking; BTX; Pt/Al_2O_3; Y zeolite

1. Introduction

The complexity of refineries has evolved over time due to an increase in market competitiveness. Heavier and hard-to-process crude oils have emerged, and the production of more clean transportation fuels has been initiated due to stringent environmental legislation. Presently, ultra-low sulfur diesel (ULSD) may contain 10 ppm sulfur, which is likely to reduce further by environmental legislation in the near future [1]. Processing of heavier crude oils generates more residual products upon distillation and causes refinery needs to conversion capacity to produce the bottom of the barrel to improve economic impact. Furthermore, yields of straight-run diesel fractions associated with the crude quality have declined drastically globally, and more low-quality feeds with higher sulfur and rich aromatics contents, such as LCO from fluid catalytic cracking units, are being blended into the streams to hydrotreaters to meet the demands of the diesel market. The boiling point of LCO is similar to that of diesel; however, its high content of polyaromatics hydrocarbons (PAH) and sulfur make it inappropriate for diesel blending [2]. The aromatic content in LCO varies from 75 to 90%, and the relative sulfur and nitrogen contents are in the range of 1.5 to 2 wt% to 750 µg/g, respectively. The cetane index of LCO lies in the range of 15 to 25, and the general physical properties of LCO have been summarized elsewhere [3, 4]. Because of these constraints, LCO is considered a low-value product as a blending stock in heavy fuel oil for viscosity adjustment or heating oil. Thus, considerable attention has been paid recently to the upgradation of such low-value LCO into a high-value product by hydrotreatment (HDT) and hydrocracking (HCK). Direct hydrocracking of LCO has been studied thoroughly over noble metals such as Pt and Pd supported by medium-acidity zeolites such as H-Y, H-Beta, and ZSM-5 [5-9]. These catalysts showed promising results of LCO conversion to naphtha and medium distillate streams with suitable composition for gasoline pools and diesel with a lower content of sulfur and aromatics. In contrast, hydrocracking of hydrotreated LCO was progressed over W-Ni-and Ni-Mo-based catalysts FC-14, FC-24, and FC-26, and the technology called FD2G [3]. An alternative technological solution for the valorization of LCO can be obtained by benzene, toluene, and xylene (BTX) by selective ring-opening of the partially hydrogenated di and tri-aromatic compounds [10]. The UOP Company has developed an LCO upgradation technology called “LCO Unicracking TM,” which can process LCO to gasoline blend stocks with a high octane number, and LCO-X technology based on selective alkyl transfer technology that can produce benzene and xylene selectively [11, 12].

Selective ring-opening can be performed on noble metals by hydrogenolysis. The hydrogenolysis activity of noble metal catalysts increases in the following order: Pt < Rh < Ir < Ru [13, 14]. Furthermore, strongly acidic, high surface area zeolites, e.g., zeolite beta, Y, etc. enhance the activity of dealkylation or C-C bond scission. Among all zeolites, Y-type zeolite is the most studied and commercially applied [15-17]. Chareonpanich et al. [18] investigated the hydrocracking of aromatic hydrocarbons such as butyl benzene, tetralin, naphthalene, 1-methyl-naphthalene, tetra-diphenylmethane, 9, 10-dihydronaphthalene, anthracene, and phenanthrene over metal-free USY zeolite at 600°C. Hydrocracking of eight aromatic hydrocarbons displayed the lowest BTX yield in the absence of the catalyst and the highest yield in the presence of USY zeolite. Furthermore, hydrocracking of tetralin as biomass tar model compounds to benzene, toluene, and xylenes over zeolites was performed under ambient conditions [19-22].

Several authors have studied the hydrocracking of individual di and tri-aromatic hydrocarbons such as naphthalene, methyl naphthalene, tetralin, anthracene, and phenanthrene. However, it is necessary to study and understand the behavior of mixed feed, which is the by-product of the refinery FCC unit. Hence, we selected the mixed feed as a model feed to simulate the LCO feed. In this context, we selected a bi-functional catalyst (a mixture of Pt/Al_2O_3 and Y zeolite) for converting di and tri-aromatic compounds (model feed) to monoaromatics.

2. Experimental

2.1 Preparation of Y Zeolite Extrudates

The Al_2O_3 precursor for binder G-300 was received from M/S. BASF GMBH and the Y zeolite powders in the H-form (CBV 712: SiO_2/Al_2O_3–12 and CBV 780: SiO_2/Al_2O_3–80) were purchased from Zeolyst International Pvt. Ltd. The Y zeolite extrudates were prepared using a zeolite/binder ratio 70:30 wt%. The extrudates were prepared using a laboratory stainless steel extruder. The obtained final extrudates were dried at room temperature for 12 h, oven-dried at 120°C for 12 h, and finally calcined at 540°C for 6 h under airflow.

2.2 Pt/Al_2O_3 Catalyst Preparation

The Pt/Al_2O_3 (0.6 wt%) catalyst was synthesized by the incipient wet impregnation method on Al_2O_3 spheres (from Sasol GMBH, 2 mm). Before impregnation, alumina spheres were dried at 110°C overnight. Next, an appropriate volume of H_2PtCl_6 solution (Sigma-Aldrich) was dispersed on dried Al_2O_3 spheres. The impregnated wet catalyst was dried at 110°C overnight and finally calcined at 550°C for 8 h under airflow.

2.3 Catalyst Characterization

Textural properties of catalysts were determined by adsorption/desorption isotherms at -196°C on Micromeritics 3 Flex. Before measurement, the sample was degassed at 300°C under a vacuum for 3 h to remove moisture. The acidity of the samples was determined by performing temperature-programmed desorption of NH_3 (NH_3-TPD) experiments using the Micromeritics AutoChem II 2920 apparatus. Before analysis, the sample was pre-treated under He flow (25 mL/min) for 1 h at 500°C. Afterward, the reactor was cooled down to 100°C and absorbed with ammonia diluted in He (NH_3:He 10:90 vol%) for 1 h. The sample was flushed with He flow to remove physisorbed ammonia

from the sample surface. Next, the temperature was linearly increased to 550°C at a rate of 10°C/min and desorbed ammonia was measured simultaneously using a thermal conductive detector (TCD). X-ray powder diffraction (XRD) patterns of zeolite samples were recorded using a benchtop MiniFlex 600, Rigaku instrument with Kβ foil filtered Cu Kα radiation at 40 kV voltage and 15 mA current. Samples were scanned at 3°/min over 2θ angles ranging from 5° to 80°. The Pt/A O_3 sample was analyzed using aberration-corrected STEM with a Jeol ARM200F (200 kV) FEG-TEM/STEM microscope equipped with a CEOS Cs-corrector on the illumination system. High-angle annular dark-field scanning transmission electron microscopy (HAADF-STEM) images were acquired by aberration-corrected STEM. The probe current used in the STEM mode was 23.2 pA using a condenser lens aperture size of 40 microns. The HAADF images were registered using a camera length of 80 mm and a collection angle of 50 to 180 mrad.

2.4 Feed Preparation

To prepare the simulated model feed decane (>99.5%), propyl benzene (>99.5%), naphthalene (>99.5%), 2-methyl naphthalene (98%), 1-methyl naphthalene (99%), anthracene (99.9%), and phenanthrene (99.9%) were purchased from Sigma-Aldrich.

2.5 Catalyst Testing

Experiments were performed in a continuous down flow isothermal fixed bed reactor having a 6.35 mm stainless steel tube reactor. The Pt/Al_2O_3 and Y zeolite catalysts were sieved (120-160 μm) and mixed. The mixed catalyst particles were loaded into the reactor at the isothermal zone. The above and below of the catalyst bed were filled with silicon carbide. Before the reaction, the catalyst was reduced at 400°C for 4 h under hydrogen gas. The liquid feed was injected into the reactor using a Gilson liquid pump, and the gaseous flows were maintained by mass flow controllers. The experiments were performed at 450 and 500°C, WHSV of 0.7 and 1.3 h^{-1}, Y zeolite SAR of 12 and 80, Pt/Al_2O_3 and Y zeolite ratios (1:1 and 1:2wt%), and paraffin concentration 5 and 20wt%. The feed and products were analyzed using gas chromatography coupled with mass spectrometry. The gas chromatography–mass spectrometry (GC-MS) was equipped with an Agilent DB-1 column of dimensions 60 m (length) × 0.32 mm (ID) × 0.25 μm (film thickness) and quadrupole mass analyzer (Agilent 5973N). All compounds were identified using the NIST mass spectral library software (NIST 14, software version: 2.2). All identified compounds in the product were grouped into mono, diaromatics, triaromatics, cyclics (naphthenes), and paraffins. The conversion and yield were calculated using the following equations:

Conversion:$(C_{\text{Feed n-decane}}-C_{\text{Effluent n-decane}})/(C_{\text{Feed n-decane}})*100$
$(C_{\text{Feed propylbenzene}}-C_{\text{Effluent propylbenzene}})/(C_{\text{Feed propylbenzene}})*100$
$(C_{\text{Feed naphthalene}}-C_{\text{Effluent naphthalene}})/(C_{\text{Feed naphthalene}})*100$
$(C_{\text{Feed 1-methylnaphthalene}}-C_{\text{Effluent 1-methylnaphthalene}})/(C_{\text{Feed 1-methylnaphthalene}})*100$
$(C_{\text{Feed 2-methylnaphthalene}}-C_{\text{Effluent 2-methylnaphthalene}})/(C_{\text{Feed 2-methylnaphthalene}})*100$
$(C_{\text{Feed anthracene}}-C_{\text{Effluent anthracene}})/(C_{\text{Feed anthracene}})*100$
$(C_{\text{Feed phenanthrene}}-C_{\text{Effluent phenanthrene}})/(C_{\text{Feed phenanthrene}})*100$

Yields: Total group compounds in wt%/feed converted in wt%
For example, total monoaromatics in wt%/feed converted in wt%

3. Results and Discussion

3.1 Catalyst Characterization

3.1.1 XRD

The XRD patterns of Pt/Al_2O_3 and γ-Al_2O_3 are shown in Figure 1A. The diffraction pattern of Pt/Al_2O_3 catalyst was similar to those of γ-Al_2O_3. The diffraction peaks for platinum oxide ($2\theta = 39.7°$, 46°, and 67.5°) were not visible, which could be due to the very small size of Pt oxide crystallites and which were well dispersed on the surface of γ-Al_2O_3 [23].

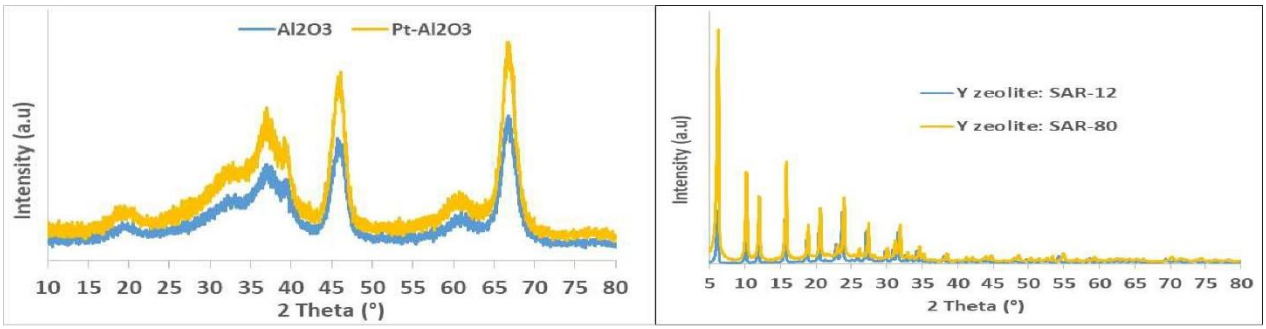

Figure 1 XRD patterns of (A) Al_2O_3, Pt/Al_2O_3, (B) Y zeolite SAR-12 and 80 catalysts.

The XRD patterns for Y zeolite SAR-12 and 80 (Figure 1B) exhibited the typical characteristics of faujasite structure with good crystallinity. The typical peaks appeared at 2θ values of 6.19°, 10.11°, 11.86°, 15.61°, 18.64°, 20.3°, 23.58°, 26.97°, 30.66°, 31.31°, 33.99,° and 34.58°.

3.1.2 Textual Properties

The textural properties of catalysts are given in Table 1. The observed pore volumes (Vp) for Pt/Al_2O_3 catalyst and SA were 0.63 cm^3/g and 168 m^2/g, respectively. The measured surface areas and total pore volume for both Y zeolites were almost similar (~710 m^2/g and 0.46 cm^3/g). Interestingly, the micropore volume reduced to around 17%, with an increase in the silica-alumina ratio from 12 to 80 without affecting the total pore volume. This could be due to different SAR of zeolites. At a lower SAR ratio, a decrease in the volume was attributed to the formation of Al oxide species, i.e., extra-framework species [24]. Pt/Al_2O_3 catalyst showed a completely mesoporous structure, whereas Y zeolites were microporous. Y zeolites had a high surface area than the Pt/Al_2O_3 catalyst.

Table 1 Textural and acidic properties of Pt/Al_2O_3 and Y zeolite (SAR 12 and 80) catalysts.

Sample	Surface area (m^2/g)	Pore volume (cm^3/g)	Micro pore volume (cm^3/g)	Pore diameter (Å)	At 180°C (mmol/g) Weak	At 350°C (mmol/g) Strong	Total acidity (mmol/g)	Weak/ strong
Pt/Al_2O_3	168	0.63	0.0006	149	1.3	0.4	1.7	3.25

Y zeolite SAR:12	719	0.46	0.25	69.4	24	9.8	33.8	2.4
Y zeolite SAR:80	707	0.47	0.20	61.2	9.9	4.7	14.6	2.1

Figure 2A, Figure 2B, and Figure 2C show HAADF-STEM images of Pt/Al_2O_3 catalyst. The surfaces of certain agglomerates of support particles exhibited increased image contrast (Figure 2A). HAADF-STEM images of initial catalysts demonstrated that Pt had highly atomically dispersed, small clusters up to 1.7 nm in diameter.

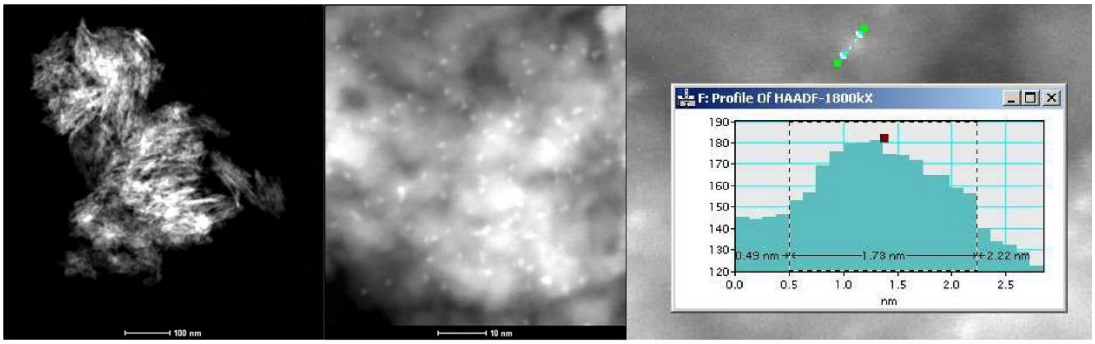

Figure 2 HAADF–STEM (A, B) images and the Pt particle size distribution (C).

The NH_3-TPD technique was used to measure the nature and number of acid sites present on Y zeolite materials, as shown in Figure 3. The profile showed that desorption occurred for all catalysts in the temperature range of 100 to 550°C. The desorption peaks from 150 to 200°C corresponded to weak acid sites, and peaks from 300 to 500°C were related to medium and strong acid sites. The desorption pattern displayed that SAR-12 had more intensity than SAR-80. These results indicated that acidity decreased at a higher SAR-80 sample. Another important finding was that the medium and strong desorption peaks were shifted to high temperatures for SAR-12 compared with SAR-80. These results indicated that the strength of medium and strong acid sites increased the total acidity of catalysts (Table 1). The total acidity was high (33.8 mmol/g) for Y zeolite with SAR-12 compared to SAR-80 (14.6 mmol/g), which is due to the lower SAR. In contrast, Pt/Al_2O_3 showed a total acidity of 1.7 mmol/g.

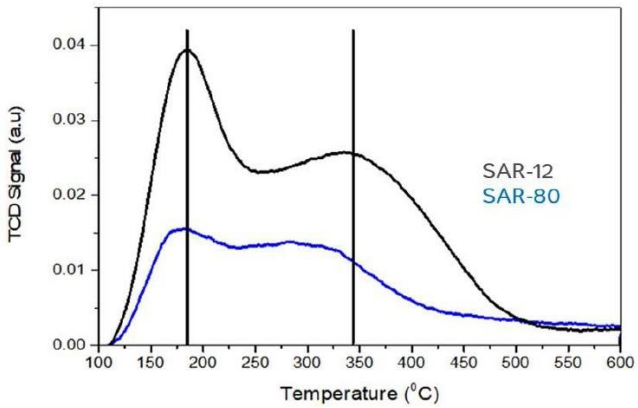

Figure 3 NH3-TPD results of Y zeolite with SAR-12 and SAR-80.

3.2 Hydrocracking of Model Feed

Hydrocracking occurred on dual-function catalysts that had hydrogenation–dehydrogenation function and cracking function. Kumar et al. [25] studied the mechanistic kinetic modeling of the hydrocracking of complex feedstocks such as vacuum gas oils. They described reaction pathways for paraffinic, naphthenic, and aromatic species over dual-functional catalysts. Hydrocracking of polynuclear aromatics involves sequential hydrogenation of aromatic rings, along with parallel or subsequent isomerization, cracking, and ring-opening steps. The present study emphasized on hydrocracking of a mixture of model feed over Pt/Al_2O_3 and Y zeolite catalysts. The detailed composition of the model feed is summarized in Table 2.

Table 2 Feed composition of model feed

S.No	Compound	Feed-A wt%	Feed-B wt%
1	n-Decane	5	25
2	Propylbenzene	28	20
3	Naphthalene	32	25
4	1-Methyl naphthalene	18	10
5	2-Methyl naphthalene	12	15
6	Phenanthrene	3	3
7	Anthracene	2	2

3.2.1 Effect of Temperature

The conversion of model feed (B) components and product selectivity from hydrocracking over a bi-functional catalyst (Pt/Al_2O_3 and Y zeolite (SAR-80)) as a function of reaction temperature are shown in Figure 4A and B, respectively. These results illustrated that the conversion trend for different components was as follows: triaromatics conversion > diaromatics conversion > monoaromatics > paraffins. The results showed that the complete conversion occurred for tri-aromatics at both temperatures. Naphthalene and 1-methyl naphthalene were converted to about 70 to 80%, whereas 2-methyl naphthalene was only converted to about 35 to 40%. The lower conversion rate of 2-methyl naphthalene could be ascribed to resonance stabilization and isomerization of 1-methyl naphthalene to 2-methyl naphthalene in the presence of acid functionality. In addition, with increasing reaction temperature from 450 to 500°C, the conversion of n-decane increased. The product distribution indicated that at 450°C, the desired 1-ring monoaromatics, 2-ring monoaromatics, and 3-ring monoaromatics were significantly formed in comparison to that at 500°C. These results demonstrated that 450°C is the optimum temperature for the formation of desired compounds. The decrease observed in aromatics and increase in naphthenes at higher temperatures could be attributed to further hydrogenation of aromatics. Overall, the BTX yields at 450, and 500°C temperatures were 29% and 11.8%, respectively. In contrast, the total monoaromatics-1 ring compounds were 43.5% and 18.1%, respectively. The detailed product distribution of GC-MS results is presented in the appendix.

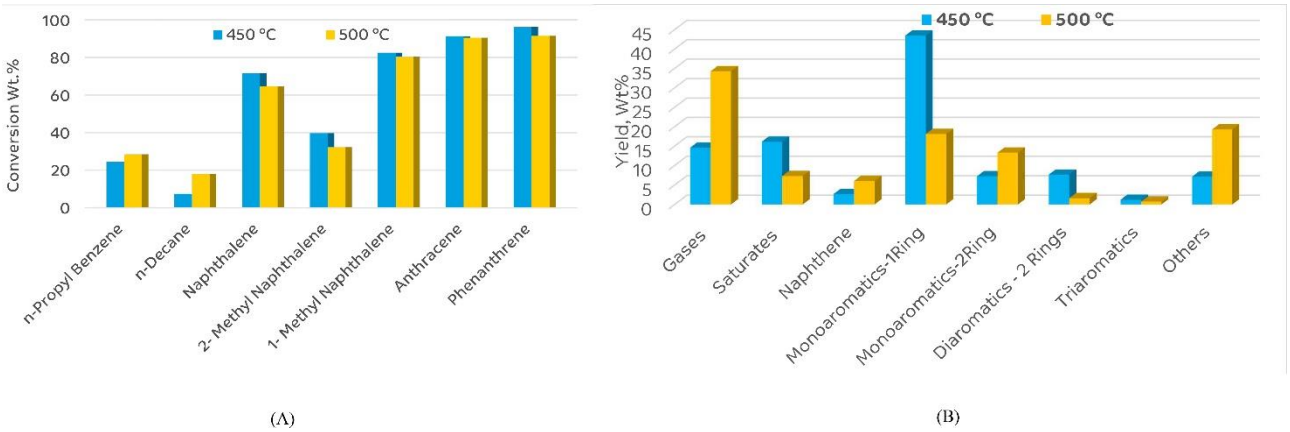

Figure 4 (A) Effect of temperature on components conversion and (B) product distribution.

Reaction conditions: Catalyst: Pt/Al_2O_3 and Y zeolite (SAR-80) (1:1wt%), WHSV-0.7 h^{-1}, pressure-60 bar, H_2/HC-10 (hydrogen/hydrocarbon mol ratio), and TOS-22 h.

3.2.2 Effect of Space Velocity

The effect of WHSV on (feed-B) conversion and distribution of different products are illustrated in Figure 5. The conversion of paraffin, monoaromatics, diaromatics, and triaromatics was high at WHSV of 0.7 h^{-1} in comparison with that at 1.3 h^{-1}. At lower WHSV, the contact time of reactants at the catalyst surface was more, resulting in high conversion. Tri-aromatic compounds such as phenanthrene and anthracene showed higher conversion in comparison with di-aromatics compounds (naphthalene, 1-methyl naphthalene, and 2-methyl naphthalene). In addition, diaromatics compounds exhibited higher conversion than monoaromatics and paraffin compounds. The difference in the activity was due to the different resonance energies of the aromatic group. The resonance energy of aromaticity followed the order: monoaromatics < diaromatics < triaromatic compounds. The resonance energy or aromaticity of different rings infused different multi-ring aromatic systems [26]. Overall, triaromatics conversion was around 90 to 100%, and diaromatics compounds conversion was around 70 to 80% at WHSV of 0.7 h^{-1}. However, very low conversion of 2-methylnaphthalene was noticed under these conditions. The presence of methyl substitution on the aromatic ring is known to stabilize the adsorbed π complex, resulting in a higher energy barrier to aromatic hydrogenation. In addition, the electronic effect of this particular structure could be responsible for lower reactivity (the lower conversion of 2-methylnaphthalene) [27]. Furthermore, the presence of acid catalyst favored isomerization of 1 and 2-methyl naphthalene. It is important to stress that for increasing the HCK yield resulted high yields of BTX formation (29% at 0.7 h^{-1} vs 10.5% at 1.3 h^{-1}).

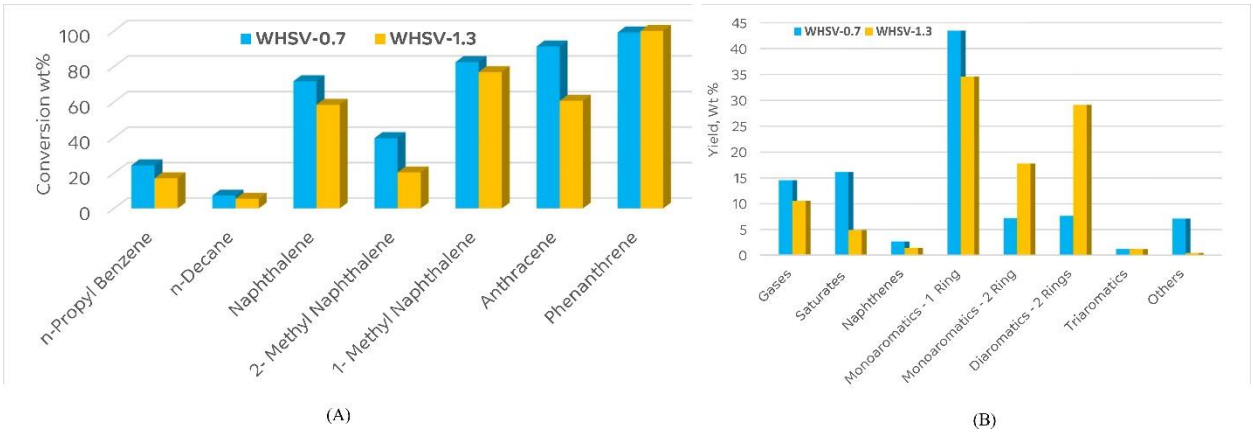

Figure 5 Effect of WHSV on model feed conversion (Figure 5A) and (Figure 5B) product distribution. Reaction conditions: catalyst: Pt/Al_2O_3 and Y zeolite (SAR-80) (1:1wt%), temp = 450°C, pressure = 60 bar, H_2/HC = 10.

The reaction pathways for the production of BTX from diaromatic compounds are shown in Scheme 1. The liquid analysis by GC-MS revealed the major products in monoaromatics-1 ring group to be benzene, toluene, xylenes, ethyl benzene, and butyl benzene. Monoaromatic-2 ring compounds majorly consisted of tetralin and methyl tetralin compounds. Diaromatics-2-ring compounds majorly comprised 2,3 dimethyl naphthalene and its isomers. In contrast, gaseous compounds included methane, ethane, propane, and butanes.

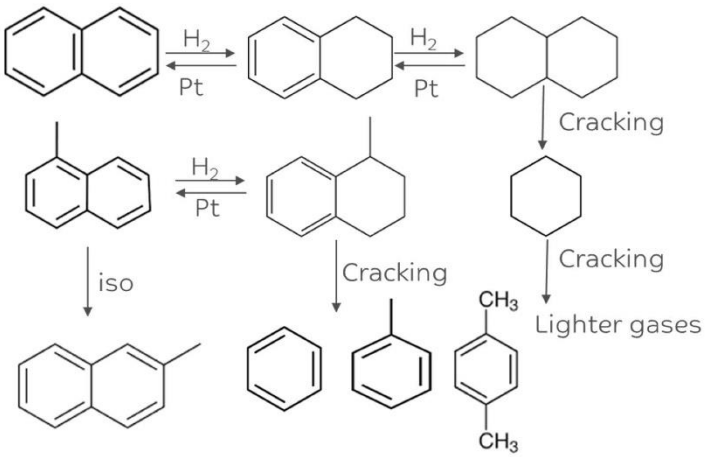

Scheme 1 Plausible routes for different product distribution during hydrocracking reaction over bi-functional catalysts.

3.2.3 Effect of Pt/Al_2O_3 and Y Zeolite Ratio

To understand the ratio between hydrogenation activity and cracking activity of bi-functional hydrocracking catalyst, reactions were performed over feed-A by varying the Pt/Al_2O_3 and Y zeolite weight ratio from 1:1 (wt%) to 1:2 (wt%) (Figure 6).

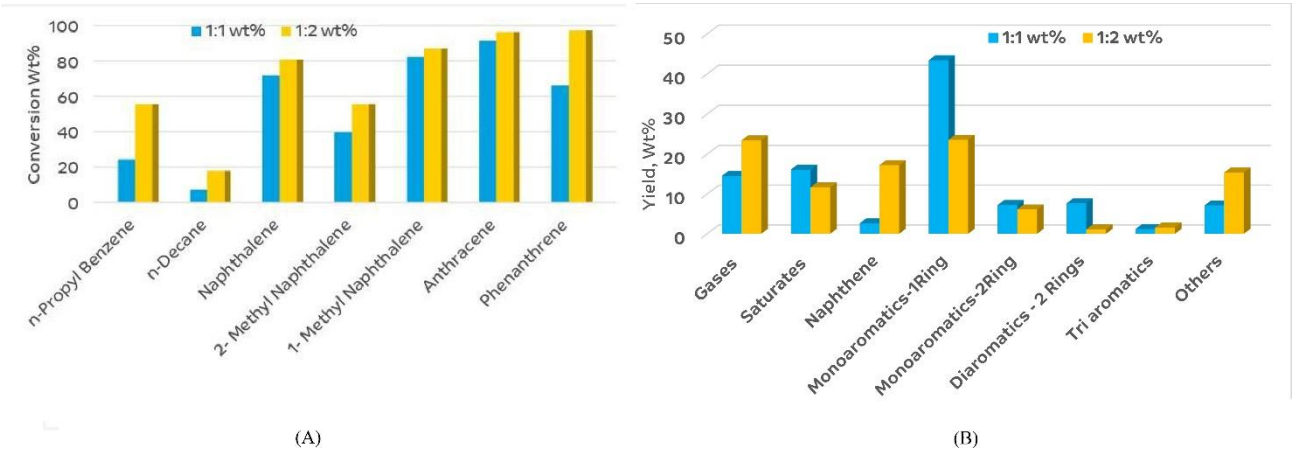

Figure 6 Effect of Pt/Al_2O_3 and Y zeolite wt% on components conversion (Figure 6A) and product distribution (Figure 6B). Reaction conditions: temperature-450°C, WHSV-0.7 h^{-1}, pressure-60 bar, H_2/HC-10, TOS-22 h.

Figure 6 results show that with an increase in the cracking functionality (increasing zeolite ratio) of the bi-functional catalyst, the feed components conversion increased significantly. More than 90% of triaromatic conversion was obtained along with increased selectivity of naphthenes in the presence of high zeolite ratios. This is consistent with earlier published results by Appleby et al. [27]. In general, changes in the zeolite content exert a more significant impact on the activity and selectivity in cracking reactions. Hydrogenation activity increased the total liquid product yield due to a larger volume of hydrogenation products. In contrast, a higher zeolite content hydrocracking catalyst showed higher selectivity for naphtha and gaseous products [28]. The higher conversion rates at high zeolite content catalysts could be due to the facilitation of more acid centers for the reaction. Furthermore, changing the hydrogenation functionality and cracking functionality had a remarkable effect on product distribution. Bi-functional catalysts with more cracking functionality displayed a higher formation of gaseous compounds and naphthenes. The higher formation of naphthenes (7.4wt% against 2wt%) at a higher zeolite content sample could be due to the fact that the Y zeolite catalyst showed not only hydrocracking but also hydrogenation function at high temperatures (>400°C) and high hydrogen pressure [29]. Normally, the catalyst with more acid sites should crack naphthenes to paraffins. On the contrary, present results showed irreversible trends. Most importantly, the decrease in the number of monoaromatic-2 ring compounds at a higher zeolite content sample (Pt/Al_2O_3 and Y zeolite 1:2wt%) was noticed, which is attributed to the hydrogen transfer reaction. In the presence of a high zeolite content, monoaromatic-2 ring compounds were easily converted to alkyl benzene types of compounds by trans alkylation reactions [30].

3.2.4 Effect of SAR of Y Zeolite

Zeolites are widely used as catalyst support and play an important role in the hydrocracking process because they improve catalytic activity, selectivity, and stability by imparting shape selectivity [31]. The mechanism of hydrocracking indicates that the formation of mild acid sites on the catalyst surface influences the reaction rate and product selectivity [32, 33]. Thus, the effect of SAR on catalysts was studied over feed-B, and the results are elucidated in Figure 7. The conversion of polyaromatics (tri-aromatics and di-aromatics) increased with a decrease in the SAR of Y zeolite from 80 to 12, which could be ascribed to higher acidity of the catalyst (i.e., with several acid sites). These results are in good agreement with NH_3-TPD results (Figure 6). In contrast, product distribution showed that a high amount of saturates and naphthenes was observed at SAR-12 (23.5% and 10%, respectively). In addition, the formation of monoaromatic-2 ring products was high at SAR-80 in comparison with 12 (14.7% against 8.3%). It could be attributed to fewer acid sites of SAR-80 zeolite, which may not be enough for β secession of tetralin and indane kind of molecules to alkylated benzene compounds. The over-cracking at the SAR-12 zeolite catalyst system is attributed to high acidity sites, particularly strong acid sites.

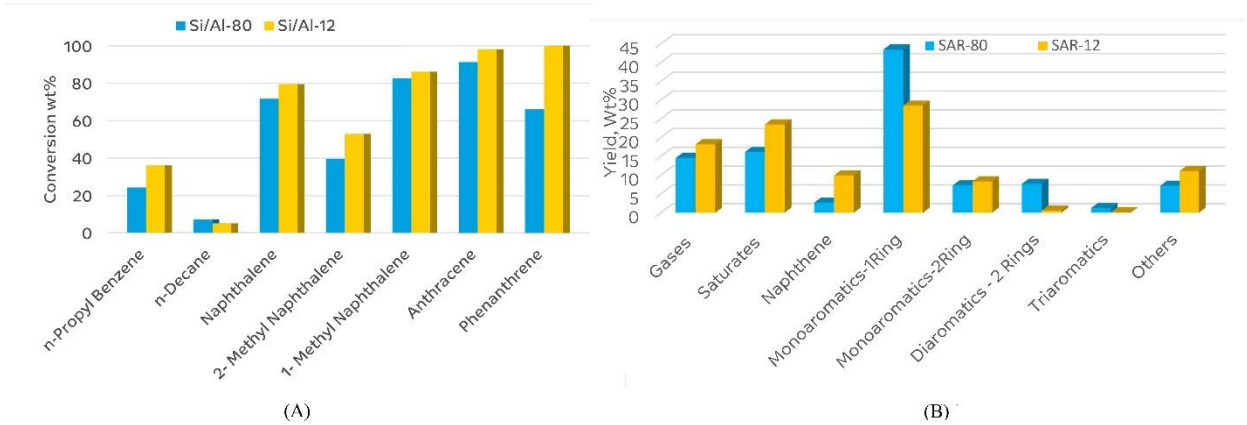

Figure 7 Effect of Si/Al of Y zeolite on component conversion (Figure 7A) and product distribution (Figure 7B). Reaction conditions: catalyst-Pt/Al_2O_3 and Y zeolite (1:1wt%), temperature-450°C, WHSV-0.7 h^{-1}, pressure-60 bar, H_2/HC-10, TOS-22 h.

3.2.5 Effect of Paraffin Concentration on the Feed

The effect of paraffin concentration on catalyst performance was studied using 5 wt% and 20 wt% paraffin concentrations in the feed (Feed-A and B, respectively, in Table 2). The results indicated that (Figure 8) paraffin concentration significantly affected the conversion of individual components. The conversion of diaromatics (naphthalene, 1-methyl naphthalene, and 2-methyl naphthalene) was 95%, 75%, and 83%, respectively, for feed B as compared to feed A. In addition, triaromatics showed complete conversion with feed B. Furthermore, significant changes in the product distribution of monoaromatic-1 ring, and gaseous compounds were noticed with feed B and with the maximum BTX yield. This effect could be due to the competitive reaction of individual components on the catalyst active sites. In addition, a high amount of paraffin in the feed allowed the formation of homogeneity of the feed mixture, which improved the diffusion of products from

the catalyst active sites. The formation of a high amount of gases in the reaction with feed B could be due to the cracking of n-decane to lighters.

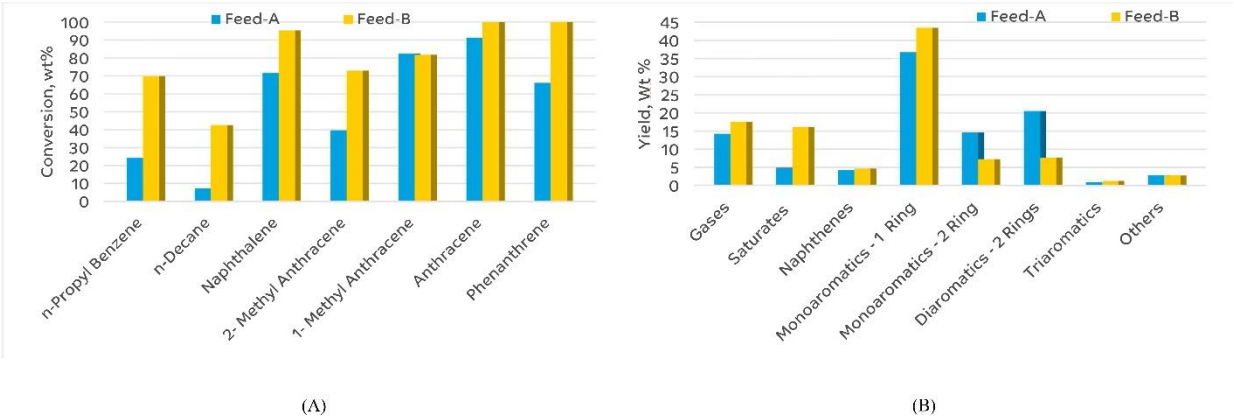

Figure 8 Effect of paraffin concentration on components conversion (Figure 8A) and product distribution (Figure 8B). Reaction conditions: Feed A and B, Pt/Al_2O_3 and Y zeolite (Si/Al-80) (1:1 wt%), temperature-450°C, WHSV-0.7 h^{-1}, pressure-60 bar, H_2/HC-10, TOS-22 h.

4. Conclusions

The bi-functional catalyst system was studied to attain a high amount of monoaromatics (BTX) from diaromatics and tri-aromatics model feed. An optimum bi-functionality such as hydrogenation and hydrocracking was achieved by changing the weight ratio of Pt/Al_2O_3, and Y zeolite as well as zeolite Si/Al ratio. In the bi-functional catalyst system, controlling hydrogenation and cracking of di and triaromatics compounds is essential to produce BTX. In this context, the catalyst system is favored by varying the Pt/Al_2O_3 and Y zeolite weight ratio. A catalyst system with 1:1 (wt/wt) of Pt/Al_2O_3 and Y zeolite produced ~36% monoaromatics by controlled hydrogenation and cracking of di-and triaromatics at an H_2 pressure of 60 bar. The effect of SAR on conversion and product selectivity was examined by selecting Y-80 and 12. At high SAR (80), selectively cracked di and tri-aromatics to desired monoaromatics (BTX). At lower SAR (12) giving over cracking of paraffins and hydrogen transfer reaction resulted in the formation of more gases and naphthenes in the product. The highest activity due to strong acid sites was evaluated using the NH_3-TPD method. At lower space velocity (0.7 h^{-1}), high conversion of paraffin, monoaromatics, diaromatics, and triaromatics was obtained; however, the activity rate for tri-aromatics was higher than for di-aromatics, which could be due to different resonance energies of the aromatic group. The selective hydrocracking conversion showed a strong dependence on catalyst ratio, SAR, temperature, WHSV, and paraffin concentration in the feed.

Author Contributions

All authors are equally contributed to the design and implementation of the research, to the analysis of the results and to the writing of the manuscript.

Competing Interests

The authors have declared that no competing interests exist.

Additional Materials

The following additional materials are uploaded at the page of this paper.

1. Table S1: GC results of product components.

References

1. Stanislaus A, Marafi A, Rana MS. Recent advances in the science and technology of ultra low sulfur diesel (ULSD) production. Catal Today. 2010; 153: 1-68.
2. Corma A, Gonzalez Alfaro VG, Orchillés AV. Decalin and tetralin as probe molecules for cracking and hydrotreating the light cycle oil. J Catal. 2001; 200: 34-44.
3. Chong P, Xuejing Y, Xiangchen F, Xinlu H, Zhenmin C, Ronghui Z, et al. Development of light cycle oil (LCO) hydrocracking technology over a commercial W-Ni based catalyst. China Pet Process Petrochem Technol. 2015; 17: 30-36.
4. Bisht D, Petri J. Considerations for upgrading light cycle oil with hydroprocessing technologies. Indian Chem Eng. 2014; 56: 321-335.
5. Gutiérrez A, Arandes JM, Castaño P, Aguayo AT, Bilbao J. Role of acidity in the deactivation and steady hydroconversion of light cycle oil on noble metal supported catalysts. Energy Fuels. 2011; 25: 3389-3399.
6. Gutiérrez A, Arandes JM, Castaño P, Olazar M, Barona A, Bilbao J. Effect of temperature in hydrocracking of light cycle oil on a noble metal-supported catalyst for fuel production. Chem Eng Technol. 2012; 35: 653-660.
7. Gutiérrez A, Arandes JM, Castaño P, Olazar M, Bilbao J. Enhancement of aromatic hydro-upgrading on a Pt catalyst by promotion with Pd and shape-selective supports. Fuel Process Technol. 2012; 101: 64-72.
8. Gutiérrez A, Arandes JM, Castaño P, Olazar M, Barona A, Bilbao J. Effect of space velocity on the hydrocracking of light cycle oil over a Pt-Pd/HY zeolite catalyst. Fuel Process Technol. 2012; 95: 8-15.
9. Gutiérrez A, Arandes JM, Castaño P, Olazar M, Barona A, Bilbao J. Preliminary studies on fuel production through LCO hydrocracking on noble-metal supported catalysts. Fuel. 2012; 94: 504-515.
10. Anilkumar M, Loke N, Patil V, Panday R. Hydrocracking of hydrotreated light cycle oil to mono aromatics over non-noble bi-functional (ni-w supported) zeolite catalysts. Catal Today. 2020; 358: 221-227.
11. Thakkar VP, Abdo SF, Gembicki VA, Mc Gehee JF. LCO upgrading - a novel approach for greater added value and improved returns. Proceedings of the National Petrochemical and Refiners Association Annual Meeting; 2005 April 5; Des Plaines, IL, USA. Des Plaines: UOP LLC.
12. Johnson JA, Frey SJ, Thakkar VP. Unlocking high value xylenes from light cycle oil. 2007. Des Plaines, IL: UOP LLC; 2007; AM-07-40.

13. Walter CG, Coq B, Figueras F, Boulet M. Competitive reaction of methylcyclohexane and n-hexane over alumina-supported platinum, iridium and ruthenium catalysts. Appl Catal A. 1995; 133: 95-102.
14. Carter JL, Cusumano JA, Sinfelt JH. Catalysis over supported metals. V. The effect of crystallite size on the catalytic activity of nickel. J Phys Chem. 1966; 70: 2257-2263.
15. Ding L, Zheng Y, Zhang Z, Ring Z, Chen J. Hydrotreating of light cycle oil using WNi catalysts containing hydrothermally and chemically treated zeolite Y. Catal Today. 2007; 125: 229-238.
16. Bataille F, Lemberton JL, Pérot G, Leyrit P, Cseri T, Marchal N, et al. Sulfided Mo and CoMo supported on zeolite as hydrodesulfurization catalysts: Transformation of dibenzothiophene and 4,6-dimethyldibenzothiophene. Appl Catal A. 2001; 220: 191-205.
17. Kunisada N, Choi KH, Korai Y, Mochida I, Nakano K. Optimum coating of USY as a support component of NiMoS on alumina for deep HDS of gas oil. Appl Catal A. 2004; 276: 51-59.
18. Chareonpanich M, Zhang ZG, Tomita A. Hydrocracking of aromatic hydrocarbons over USY-zeolite. Energy Fuels. 1996; 10: 927-931.
19. Kostyniuk A, Bajec D, Likozar B. Catalytic hydrocracking reactions of tetralin as aromatic biomass tar model compound to benzene/toluene/xylenes (BTX) over zeolites under ambient pressure conditions. J Ind Eng Chem. 2021; 96: 130-143.
20. Kostyniuk A, Bajec D, Likozar B. Catalytic hydrogenation, hydrocracking and isomerization reactions of biomass tar model compound mixture over Ni-modified zeolite catalysts in packed bed reactor. Renew Energy. 2021; 167: 409-424.
21. Kostyniuk A, Bajec D, Likozar B. Hydrocracking, hydrogenation and isomerization of model biomass tar in a packed bed reactor over bimetallic NiMo zeolite catalysts: Tailoring structure/acidity. Appl Catal A. 2021; 612: 118004.
22. Kostyniuk A, Bajec D, Prašnikar A, Likozar B. Catalytic hydrocracking, hydrogenation, and isomerization reactions of model biomass tar over (W/Ni)-zeolites. J Ind Eng Chem. 2021; 101: 293-306.
23. An N, Yuan X, Pan B, Li Q, Li S, Zhang W. Design of a highly active Pt/Al_2O_3 catalyst for low-temperature CO oxidation. RSC Adv. 2014; 4: 38250-38257.
24. Fink A, Gierlich CH, Delidovich I, Palkovits R. Systematic catalyst screening of zeolites with various frameworks and Si/Al ratios to identify optimum acid strength in OME synthesis. ChemCatChem. 2020; 12: 5710-5719.
25. Kumar H, Froment GF. Mechanistic kinetic modeling of the hydrocracking of complex feed stocks, such as vacuum gas oil. Ind Eng Chem Res. 2007; 46: 5881-5897.
26. Stanislaus A, Cooper BH. Aromatic hydrogenation catalysis: A Review. Catal Rev Sci Eng. 1994; 36: 75-123.
27. Appleby WG, Gibson JW, Good GM. Coke formation in catalytic cracking. Ind Eng Chem Process Des Dev. 1962; 1: 102-110.
28. Scherzer J, Gruia AJ. Hydrocracking science and technology. New York: Marcel Dekker; 1996. pp.103.
29. Ebitani K, Tsuji J, Hattori H, Kita H. Dynamic modification of surface acid properties with hydrogen molecule for zirconium oxide promoted by platinum and sulfate ions. J Catal. 1992; 135: 609-617.
30. Tsai TC, Liu SB, Wang I. Disproportionation and transalkylation of alkylbenzenes over zeolite catalysts. Appl Catal A. 1999; 181: 355-398.

31. Maesen TLM, Calero S, Schenk M, Smit B. Alkane hydrocracking: Shape selectivity or kinetics. J Catal. 2004; 221: 241-251.
32. Francis J, Guillon E, Bats N, Pichon C, Corma A, Simon LJ. Design of improved hydrocracking catalysts by increasing the proximity between acid and metallic sites. Appl Catal A. 2011; 409: 140-147.
33. Treacy MMJ, Higgins JB, von Ballmoos R. Collection of simulated XRD powder patterns for zeolites. New York: Elsevier; 2001. pp.148.